Lattice Boltzmann simulations of a time-dependent natural convection problem

Benoît Trouette

Lattice Boltzmann simulations of a time-dependent natural convection problem

Benoît Trouette

September 2, 2013

Abstract

A two-dimensional double Multiple-Relaxation-Time thermal lattice Boltzmann method is used to simulate natural convection flows in differentially heated cavities. The buoyancy effects are considered under the Boussinesq assumption. Flow and temperature fields are respectively solved with nine and five discrete velocities models. Boundary conditions are implemented with the classical bounce-back or a "on-node" approach. The latter uses popular Zou and He and Counter-Slip formulations. This paper evaluates the differences between the two implementations for steady and time-dependent flows as well as the space and time convergence orders.

Keywords: Thermal lattice Boltzmann method double distribution function time-dependent natural convection Richardson extrapolation convergence study

1 Introduction

The Lattice Boltzmann Method (LBM), derived from the lattice gas automata (29), has been developed as an alternative numerical scheme for solving the incompressible Navier-Stokes equations. It has demonstrated its ability to simulate several physical systems (5). Its straightforward implementation, natural parallelism and easy boundary condition treatment (4) make it very efficient and accurate for hydrodynamical flows. However, for thermal flows, its efficiency is a pending issue.

Indeed, thermal lattice Boltzmann methods can be split into three main classes. The first one relies on increasing the number of discrete velocities in order to make the original athermal LBM able to solve correctly the temperature field (1). The main disadvantages of this approach are the loss of the cellular automata transport scheme and a fixed Prandtl number. The second one is the hybrid approach. Mass and momentum are solved with a lattice Boltzmann model while the convection-diffusion equation for temperature is solved with a classic macroscopic solver like Finite-Volume or Finite-Element methods (24; 31; 22). Counterparts are an harder parallelization and the resolution of a linear system. Finally, the third one, the double distribution function

formulation uses two evolution equations: one for the mass and momentum conservation and one for the temperature (16; 11; 32). This approach preserves the natural advantages of lattice methods: the local formulation and the explicit time evolution scheme. Besides, supplementary distribution functions can be added to take into account additional effects like magnetic field (2). Mass and momentum equations can be solved with the generalized, or Multiple Relaxation Times (MRT), formulation (23; 8). Two approaches stand out for the thermal part: the internal energy formulation (18; 37) and lattice Boltzmann schemes designed for convection-diffusion equations (40). The former might be suitable for non straight boundary condition (44) and fluid-solid conjugate heat transfer (42; 30). The latter offers more flexibility in the discrete velocities set (20) and recent developments show that evolution equation can be solved with a MRT collision operator (32; 35; 34; 41).

In many cases, lattice Boltzmann method is used for stationary flows and do not enjoy the benefits of the inherent unsteady formulation. Indeed, the physical transient flow has to be simulated and calculations of accurate solutions would be very expensive compared to stationary solvers.

Considering this background, this work aims to analyze results and convergence orders of the double MRT method for a time-dependent natural convection flow configuration. Reference values are extracted from benchmark solutions on differentially heated cavities (27; 43). Proper comparisons with theoretical second-order accuracy both in space and time (5) are also made thanks to Richardson Extrapolation. Because of numerical instability, this analysis can hardly be handled using the classical LBM method with the Bhatnagar-Gross-Krook (BGK) collision term.

This paper is organized as follows. Section 2 presents the general configuration of the differentially heated cavity under Boussinesq approximation. In section 3, the numerical method is described: a double MRT lattice Boltzmann method using respectively nine and five velocities models for the fluid flow and the energy equation is detailed. The obtained results for two configurations are presented in Section 4. Comparisons with reference and convergence orders are discussed. Finally, the last section is dedicated to the concluding remarks.

2 Problem description

The configuration studied is the natural convection in a two-dimensional cavity heated differentially on vertical side walls. The configuration is illustrated in figure 1 where W is the width and H the height of the cavity. The cavity aspect ratio is $A = H/W$. The gravity vector is directed in the negative y-coordinate direction. The Boussinesq hypothesis is used and only small temperature variation from the mean temperature are admitted.

The dimensionless formulation of incompressible Navier-Stokes and energy equation coupled with Boussinesq hypothesis for time-dependent convection

problem is written:

$$\begin{cases} \boldsymbol{\nabla} \cdot \boldsymbol{u} = 0 \\ \dfrac{\partial \boldsymbol{u}}{\partial t} + \boldsymbol{u} \cdot \boldsymbol{\nabla} \boldsymbol{u} = -\boldsymbol{\nabla} p + \sqrt{\dfrac{Pr}{Ra}} \boldsymbol{\nabla}^2 \boldsymbol{u} + \theta \boldsymbol{e}_y \\ \dfrac{\partial \theta}{\partial t} + \boldsymbol{u} \cdot \boldsymbol{\nabla} \theta = \sqrt{\dfrac{1}{RaPr}} \boldsymbol{\nabla}^2 \theta \end{cases} \tag{1}$$

where $\boldsymbol{u} = (u, v)$, p and θ are respectively the velocity, pressure and temperature fields and $\boldsymbol{e}_y$ is the unit vector in the y-direction. This dimensionless system was obtained using the characteristic length W, buoyancy velocity scale $U = \sqrt{g\beta W \Delta T}$, time scale W/U and pressure scale ρU^2. Here, ρ is the mass density, g the gravitational acceleration and β the coefficient of thermal expansion. The dimensionless temperature is defined as follows:

$$\theta = \frac{T - T_{ref}}{T_h - T_c} \quad \text{with} \quad T_{ref} = \frac{T_h + T_c}{2} \tag{2}$$

and T_h and T_c are respectively the prescribed temperatures of hot and cold walls. The Rayleigh and Prandtl numbers are control parameters of the problem and are written:

$$Ra = \frac{g\beta \Delta T W^3}{\nu \alpha} \quad \text{and} \quad Pr = \frac{\nu}{\alpha} \tag{3}$$

where α is the thermal diffusivity, ν the kinetic viscosity, and $\Delta T = T_h - T_c$ the temperature difference between the hot and the cold walls. For all calculations, the Prandtl number is $Pr = 0.71$ (air at STP) and the aspect ratio A and the Rayleigh number Ra are free parameters.

The cavity boundary conditions for the velocity field are a no-slip conditions, i.e. $u = v = 0$ on all walls. On the left and right walls, the prescribed temperature boundary conditions is written:

$$\theta(x = 0, y) = +\frac{1}{2} \quad \text{and} \quad \theta(x = 1, y) = -\frac{1}{2} \tag{4}$$

Along the horizontal bottom and top walls, the zero-flux condition reads

$$\left.\frac{\partial \theta}{\partial y}\right|_{y=0} = 0 \quad \text{and} \quad \left.\frac{\partial \theta}{\partial y}\right|_{y=A} = 0 \tag{5}$$

For all calculations, solution is initialized with an isothermal fluid at rest, .i.e.

$$\boldsymbol{u}(u, v) = \boldsymbol{0} \quad \text{and} \quad \theta = 0 \tag{6}$$

Two configurations will be studied. The first one, the classical square cavity ($A = 1$) with $Ra = 10^6$, is used as a validation. In the second case, an aspect ratio $A = 8$ and a Rayleigh number $Ra = 3.4 \times 10^5$, lead to a time-dependent periodic flow, also referenced as a benchmark solution. In all cases, the Prandtl number is set at 0.71.

3 Numerical methods

We consider the double Multiple-Relaxation-Times thermal lattice Boltzmann (MRT-TLB) model introduced in (32; 35; 41). Two sets of distribution functions are used. The evolution equations for both mass and momentum and thermal distributions will be described as well as the coupling. Boundary conditions treatment will also be presented.

The general principle of lattice Boltzmann methods is the following: the phase space is discretized into a regular lattice, or mesh, and into a finite set of N symmetrical discrete velocities, $\boldsymbol{e}_{i=1,\dots,N}$. Lattice nodes are $\boldsymbol{x}_{j=1,\dots,N_x\times N_y}$ where N_x and N_y stand respectively for the number of nodes in $x-$ and $y-$directions. A set of distribution functions, associated with discrete velocities, is defined on each node. Their evolutions are governed by a free transport, associated with the discrete time step δ_t, along the discrete velocities. Then, a collision process makes the distribution functions relax through an equilibrium. During collisions, macroscopic quantities such as mass and momentum are conserved.

3.1 Multiple relaxation time method for mass and momentum

The time evolution equation for the mass and momentum conservations can be written as follows:

$$\begin{aligned}\boldsymbol{f}(\boldsymbol{x}_j+\boldsymbol{e}\,\delta_t,t+\delta_t)-\boldsymbol{f}(\boldsymbol{x}_j,t) =& -Q(\boldsymbol{f}(\boldsymbol{x}_j,t)-\boldsymbol{f}^{eq}(\boldsymbol{x}_j,t))\\ &+\boldsymbol{F}(\boldsymbol{x}_j,t)\end{aligned} \tag{7}$$

where Q is the collision matrix and $\boldsymbol{F}(\boldsymbol{x}_j,t)$ an external force. The collision matrix Q can be written in the general form:

$$Q = M^{-1}SM \tag{8}$$

and the evolution equation (7) becomes

$$\begin{aligned}\boldsymbol{f}(\boldsymbol{x}_j+\boldsymbol{e}\,\delta_t,t+\delta_t)-\boldsymbol{f}(\boldsymbol{x}_j,t) =& -M^{-1}S(\boldsymbol{m}(\boldsymbol{x}_j,t)-\boldsymbol{m}^{eq}(\boldsymbol{x}_j,t))\\ &+\boldsymbol{F}(\boldsymbol{x}_j,t).\end{aligned} \tag{9}$$

The quantities, $\boldsymbol{f}(\boldsymbol{x}_j,t)$, $\boldsymbol{f}^{eq}(\boldsymbol{x}_j,t)$, $\boldsymbol{m}(\boldsymbol{x}_j,t)$, $\boldsymbol{m}^{eq}(\boldsymbol{x}_j,t)$ and $\boldsymbol{F}(\boldsymbol{x}_j,t)$ are N-tuple vectors and the superscript eq stands for the equilibrium values. The general notation for a N-tuple vector $\boldsymbol{\phi}$ expressed at time t is:

$$\begin{aligned}\boldsymbol{\phi}(\boldsymbol{x}_j,t) &= (\phi_1(\boldsymbol{x}_j,t),\dots,\phi_N(\boldsymbol{x}_j,t))^T\\ \boldsymbol{\phi}(\boldsymbol{x}_j+\boldsymbol{e}\,\delta_t,t) &= (\phi_1(\boldsymbol{x}_j+\boldsymbol{e}\,\delta_t,t),\dots,\phi_N(\boldsymbol{x}_j+\boldsymbol{e}\,\delta_t,t))^T\end{aligned} \tag{10}$$

where T denotes the transpose matrix. The velocity distribution function $\boldsymbol{f}(\boldsymbol{x}_j,t)$ is expressed in the velocity space $\mathbb{V}=\mathbb{R}^N$ while its corresponding moment $\boldsymbol{m}(\boldsymbol{x}_j,t)$ is in the moment space $\mathbb{M}=\mathbb{R}^N$. With the above expressions, the mapping between discrete velocity space $\mathbb{V}$ and moment space $\mathbb{M}$ is

achieved by the transformation matrix M which maps the vector $\boldsymbol{f}(\boldsymbol{x}_j, t)$ to the vector $\boldsymbol{m}(\boldsymbol{x}_j, t)$:

$$\boldsymbol{m}(\boldsymbol{x}_j, t) = M\boldsymbol{f}(\boldsymbol{x}_j, t) \quad \text{and} \quad \boldsymbol{f}(\boldsymbol{x}_j, t) = M^{-1}\boldsymbol{m}(\boldsymbol{x}_j, t) \tag{11}$$

The operator M is a square matrix and its rank is equal to the number of discrete velocities N. With the $N = 9$ velocities model ($d2q9$), discrete velocities are:

$$\boldsymbol{e}_i = \begin{cases} (0,0) & i = 1 \\ (1,0)e,\ (0,1)e\ ,\ (-1,0)e\ ,\ (0,-1)e & i = 2-5 \\ (1,1)e,\ (-1,1)e,\ (-1,-1)e,\ (1,-1)e & i = 6-9 \end{cases} \tag{12}$$

where $e = \delta_x/\delta_t$, and δ_x and δ_t are the lattice spacing and discrete time steps. On the lattice, CFL consideration generally leads to $\delta_x = \delta_t = 1$.

To determine the transformation matrix M, the ordering of the moments must be prescribed first. Here, the choice is:

$$\begin{aligned} \boldsymbol{m}(\boldsymbol{x}_j, t) \equiv \boldsymbol{m} &= (m_1, m_2, m_3, m_4, m_5, m_6, m_7, m_8, m_9)^T \\ &= (\rho, j_x, j_y, e, p_{xx}, p_{xy}, q_x, q_y, \epsilon)^T \end{aligned} \tag{13}$$

where ρ is the mass density, $\boldsymbol{j} = (j_x, j_y) = \rho(u, v) = \rho\boldsymbol{u}$ is the impulsion and $\boldsymbol{u}$ is the flow velocity, e, p_{xx} and p_{xy} are second-order moments corresponding to energy, and two off-diagonal components of the stress tensor, respectively. q_x and q_y are the third-order moments corresponding to $x-$ and $y-$ components of the energy flux and ϵ is the fourth-order moment of energy square. With this ordering of the moments, the transformation matrix can be constructed thanks to the Gram-Schmidt orthogonalization (24):

$$M = \begin{bmatrix} 1 & 1 & 1 & 1 & 1 & 1 & 1 & 1 & 1 \\ -4 & -1 & -1 & -1 & -1 & 2 & 2 & 2 & 2 \\ 4 & -2 & -2 & -2 & -2 & 1 & 1 & 1 & 1 \\ 0 & 1 & 0 & -1 & 0 & 1 & -1 & -1 & 1 \\ 0 & -2 & 0 & 2 & 0 & 1 & -1 & -1 & 1 \\ 0 & 0 & 1 & 0 & -1 & 1 & 1 & -1 & -1 \\ 0 & 0 & -2 & 0 & 2 & 1 & 1 & -1 & -1 \\ 0 & 1 & -1 & 1 & -1 & 0 & 0 & 0 & 0 \\ 0 & 0 & 0 & 0 & 0 & 1 & -1 & 1 & -1 \end{bmatrix} \tag{14}$$

M being an orthogonal matrix, its inverse can be computed according to the formula: $M^{-1} = M^T(MM^T)^{-1}$. In the case of an isothermal fluid, the conserved variables are only the density ρ and the momentum $\boldsymbol{j}$. The other moments are non-conserved moments and as suggested in Ref. (24), they relax linearly towards their equilibrium values. For the $d2q9$ model, the non-conserved moments

$(i = 4 - 9)$ are:

$$\begin{aligned} m_4^{eq} &= e^{eq} = -2\rho + 3\rho_0 \boldsymbol{u} \cdot \boldsymbol{u} \\ m_5^{eq} &= p_{xx}^{eq} = \rho_0(u^2 - v^2) \\ m_6^{eq} &= p_{xy}^{eq} = \rho_0 uv \\ m_7^{eq} &= q_x^{eq} = -\rho_0 u \\ m_8^{eq} &= q_y^{eq} = -\rho_0 v \\ m_9^{eq} &= \epsilon^{eq} = \rho - 3\rho_0 \boldsymbol{u} \cdot \boldsymbol{u} \end{aligned} \tag{15}$$

where the constant ρ_0 is the mean density in the system. With the above equilibrium moments, the sound speed of the lattice is $c_s = 1/\sqrt{3}$. As mentioned, the collision process makes the moments relax towards their equilibrium values as follows:

$$\boldsymbol{m}^c = \boldsymbol{m} - S(\boldsymbol{m} - \boldsymbol{m}^{eq}) \tag{16}$$

where superscript c denotes the post-collision state and S is the diagonal relaxation matrix. The post-collision vector $\boldsymbol{f}^c$ is then carried out as

$$\boldsymbol{f}^c = \boldsymbol{f} - Q(\boldsymbol{f} - \boldsymbol{f}^{eq}). \tag{17}$$

The diagonal matrix S is given by

$$S = \mathrm{diag}(1, 1, 1, s_e, s_\nu, s_\nu, s_q, s_q, s_\epsilon) \tag{18}$$

where $s_i \in (0, 2)$ for the non-conserved moments. The choice of the relaxation parameters s_i can be determined by a linear stability analysis (23). In this work, as suggested by (28) we will use

$$s_\nu = s_e = s_\epsilon = \frac{2}{6\nu + 1} \quad \text{and} \quad s_q = 8\frac{2 - s_\nu}{8 - s_\nu} \tag{19}$$

That leads to the Two-Relaxation Time (TRT) model (15). Let's note that, based on the product $\Lambda = \left(\frac{1}{s_\nu} - \frac{1}{2}\right)\left(\frac{1}{s_q} - \frac{1}{2}\right)$, the current choice gives $\Lambda = 3/16$ and leads to correct positions of walls when bounce-back boundary conditions are used. Other choices are possible. For example, $\Lambda = 1/4$ leads to a better stability of the LBM and provides steady-state solutions dependant only on the equilibrium function (14; 13). Values $\Lambda = 1/6$ and $1/12$ respectively remove high-order diffusion and advection errors. The choice $s_i = 1/\tau_{BGK}$ recovers the single relaxation time or Bhatnagar-Gross-Krook (BGK) model (3). Thanks to this MRT formulation, the different models for the collision process can be tested only by changing the values of the relaxation coefficients.

The macroscopic fluid variables density ρ and velocity $\boldsymbol{u}$ are obtained from the moments of the distribution functions as follows:

$$\rho = \sum_{i=1}^{9} f_i \quad \text{and} \quad \rho_0 \boldsymbol{u} = \sum_{i=1}^{9} \boldsymbol{e}_i f_i \tag{20}$$

The corresponding form of the equilibrium distribution is given by the formula (23):

$$f_i^{eq} = w_i \rho \left(1 + 3(\boldsymbol{e}_i \cdot \boldsymbol{u}) + \frac{9}{2}(\boldsymbol{e}_i \cdot \boldsymbol{u})^2 - \frac{3}{2}\boldsymbol{u}^2 \right) \tag{21}$$

where $\omega_1 = 0$, $\omega_{2-4} = 1/9$ and $\omega_{5-9} = 1/36$ are lattice constants. This particular form of the equilibrium distribution function is related to the incompressible formulation of the Navier-Stokes equations (17). This expression will be useful when formulating the boundary conditions.

3.2 Multiple relaxation time method for thermal problem

The same way, the energy conservation is modelled by an evolution equation. The distribution functions, noted $\boldsymbol{g}$, obey to the following equation:

$$\boldsymbol{g}(\boldsymbol{x}_j + \boldsymbol{e}\,\delta_t, t + \delta_t) - \boldsymbol{g}(\boldsymbol{x}_j, t) = -Q(\boldsymbol{g}(\boldsymbol{x}_j, t) - \boldsymbol{g}^{eq}(\boldsymbol{x}_j, t)) \tag{22}$$

The corresponding lattice has now five discrete velocities, and reads:

$$\boldsymbol{e}_i = \begin{cases} (0,0) & i = 1 \\ (1,0)e,\ (0,1)e,\ (-1,0)e,\ (0,-1)e & i = 2-5 \end{cases} \tag{23}$$

Like in the previous section, Q represents the collision operator $Q = M^{-1}SM$, and the transformation matrix is given by

$$M = \begin{bmatrix} 1 & 1 & 1 & 1 & 1 \\ 0 & 1 & 0 & -1 & 0 \\ 0 & 0 & 1 & 0 & -1 \\ -4 & 1 & 1 & 1 & 1 \\ 0 & 1 & -1 & 1 & -1 \end{bmatrix}. \tag{24}$$

Like the dynamic part, this matrix is invertible and orthogonal. The temperature θ is the only conserved quantity and can be computed by:

$$\theta = \sum_{i=1}^{N} g_i \tag{25}$$

The equilibrium moments, $\boldsymbol{m}^{eq}$ corresponding to the distribution functions $\boldsymbol{g}$, can be written as:

$$m_1^{eq} = \theta, \quad m_2^{eq} = u\theta, \quad m_3^{eq} = v\theta, \quad m_4^{eq} = a\theta, \quad m_5^{eq} = 0 \tag{26}$$

where $\boldsymbol{u} = (u, v)$ is the macroscopic computed velocity and a is a constant. The diagonal relaxation matrix is given by:

$$S = \mathrm{diag}(1, s_\alpha, s_\alpha, s_e, s_\nu) \tag{27}$$

The choice of s_i is discussed in details in (41). We take here

$$\frac{1}{s_e} - \frac{1}{2} = \frac{1}{s_\nu} - \frac{1}{2} = \frac{1}{6} \quad \text{and} \quad \frac{1}{s_\alpha} - \frac{1}{2} = \frac{\sqrt{3}}{6} \tag{28}$$

Theses parameters lead to the thermal diffusivity

$$\alpha = \frac{\sqrt{3}(4+a)}{60} \tag{29}$$

where the constant a must be maintained $a < 1$ in order to avoid numerical instability of the $d2q5$ model. The value of a will be determined with the physical problem parameters and will be discussed in section 3.5.

The corresponding form of the equilibrium for the distribution functions $\boldsymbol{g}$ is given by the formula

$$g_i^{eq} = \omega_i \theta \left(1 + 3\boldsymbol{e}_i \cdot \boldsymbol{u}\right) \tag{30}$$

where $\omega_1 = 0$ and $\omega_{2-5} = 1/4$ are $d2q5$ lattice constants.

3.3 External forcing

In a natural convection problem under Boussinesq hypothesis, the external forcing represents the buoyancy effect. In the coordinate system, this force is given by

$$\boldsymbol{F}(\boldsymbol{x}_j, t) = \boldsymbol{F} = f\boldsymbol{e}_y \quad \text{with} \quad f = -\rho_0 \beta g \theta \Delta T \tag{31}$$

The projection of $\boldsymbol{F}$ on the velocity space related to mass and momentum conservation is given by:

$$F_i = -3\omega_i f \frac{\boldsymbol{e}_i \cdot \boldsymbol{e}_y}{c^2} \tag{32}$$

A brief review of force term implementations and their consequences in lattice Boltzmann model can be found in (33).

3.4 Boundary conditions

Two popular kinds of boundary conditions (BCs) are used to impose the macroscopic conditions on velocity and thermal fields described in Sec. 2. The first implementation uses the bounce-back, or anti bounce-back, conditions for both velocity and thermal fields (BB-BCs). With this method, the position of physical walls is half a lattice spacing beyond the last fluid node. The second formulation uses Zou and He (45) implementation for the velocity field and a Counter-Slip approach for thermal field (21; 10). This particular choice is noted ZHCS-BCs in the following. A review of common implementation of boundary conditions for advection-diffusion models can be found in (20). Both methods are then briefly described.

Two remarks are in order here: 1) With BB-BCs, physical walls are not on nodes but halfway beyond the last fluid node. Then ,the use of a multiple relaxation time model (MRT or TRT) is strongly recommended (41). Indeed, with the BGK model, the boundary location depends on the single relaxation time τ_{BGK}. 2) As a consequence, with N fluid nodes, the domain length in lattice units is N when BB-BCs are used and $N-1$ with ZHCS-BCs.

3.4.1 Bounce-back approach

As mentioned, when the bounce-back scheme is applied, the effective boundaries in the $x-$direction are in $x = 1/2$ and $x = N_x + 1/2$. No-slip boundary conditions are then realized by the bounce-back scheme. The incoming unknown distribution function $f_j(\boldsymbol{x}_f, t+\delta_t)$ is equal to the outgoing post-collision distribution function $f_i^c(\boldsymbol{x}_f, t)$:

$$f_{\bar{i}}(\boldsymbol{x}_f, t+\delta_t) = f_i^c(\boldsymbol{x}_f, t) \tag{33}$$

where $\boldsymbol{x}_f$ is a fluid node adjacent to a boundary and the incoming distribution function $f_{\bar{i}}$ corresponds to $\boldsymbol{e}_{\bar{i}} = -\boldsymbol{e}_i$.

For the temperature field, a bounce-back like scheme can also be applied (41). For a wall at a fixed temperature θ_w, the following boundary condition is used:

$$g_{\bar{i}}(\boldsymbol{x}_f, t+\delta_t) = -g_i^c(\boldsymbol{x}_f, t) + 2\sqrt{3}\,\alpha\,\theta_w \tag{34}$$

An adiabatic wall can be realized with the anti bounce-back condition:

$$g_{\bar{i}}(\boldsymbol{x}_f, t+\delta_t) = g_i^c(\boldsymbol{x}_f, t) \tag{35}$$

3.4.2 Zou-He and Counter-Slip boundary conditions

For the dynamic part, the no-slip condition for the velocity field is imposed by Zou and He formulation (45). This approach relies on the bounce-back rule for non-equilibrium part of the distribution functions. For thermal counterpart, fixed temperature or zero-flux are set with a Counter-Slip approach (11; 10). The incoming unknown distributions are assumed to be at the equilibrium. Both approaches are consistent with the second-order accuracy (26). Derivation of boundary conditions is not presented here. The implementation and the particular treatment for corners can be found in the following references (21; 45; 26; 39). Let us underline that this "on-node" approach allows to impose more sophisticated boundary conditions like pressure boundary conditions for the dynamic part and non-zero fluxes for the thermal part. Furthermore, this formulation is more portable and can also be used with the internal energy formulation method that uses $d2q9$ model to simulate the thermal effects (37; 9).

It is important to remind that the choice of boundary conditions defines the size of the computational domain and, as a consequence, the physical space step.

3.5 Problem set-up

Setting up a problem in lattice Boltzmann method is not always obvious and some cautions must be taken before each simulation.

The results are generally presented in dimensionless units. Then, we need to convert values obtained on the lattice (in lattice units). The procedure presented here resumes the general procedure given in Ref. (25). In dimensionless formulation, conservation of mass, momentum and energy is given by system (1). Using

a Chapmann-Enskog procedure (12), evolution equations (7) and (22) lead to the following approached system:

$$\begin{cases} \boldsymbol{\nabla}_L \cdot \boldsymbol{u}_L = 0 \\ \dfrac{\partial \boldsymbol{u}_L}{\partial t_L} + \boldsymbol{u}_L \cdot \boldsymbol{\nabla}_L \boldsymbol{u}_L = -\boldsymbol{\nabla}_L p_L + \nu_L \boldsymbol{\nabla}_L^2 \boldsymbol{u}_L + f_L \boldsymbol{e}_y \\ \dfrac{\partial \theta_L}{\partial t_L} + \boldsymbol{u}_L \cdot \boldsymbol{\nabla}_L \theta_L = \alpha_L \boldsymbol{\nabla}_L^2 \theta_L \end{cases} \tag{36}$$

In this section, values with subscript L denotes lattice values while classic notation stands for dimensionless ones. The following scalings are used to express system (1) on the lattice

$$\boldsymbol{x} = \delta_x \boldsymbol{x}_L, \quad t = \delta_t t_L, \quad \boldsymbol{u} = \frac{\delta_x}{\delta_t} \boldsymbol{u}_L, \quad p = \rho_0 \frac{\delta_x^2}{\delta_t^2} p_L \tag{37}$$

The lattice parameters can then be identified and related to dimensionless parameters Ra, Pr, δ_x and δ_t:

$$\nu_L = \sqrt{\frac{Pr}{Ra}} \frac{\delta_t}{\delta_x^2}, \quad \alpha_L = \sqrt{\frac{1}{RaPr}} \frac{\delta_t}{\delta_x^2} \quad \text{and} \quad f_L = \frac{\delta_t^2}{\delta_x} f \tag{38}$$

However, in lattice Boltzmann simulations, it is rather convenient to work with the Mach number Ma defined by $Ma = U/c_s$ where U is a reference velocity and c_s is the sound speed. Using $\sqrt{g\beta\Delta T L}$ as a reference velocity, we obtain on the lattice the following relation:

$$\nu_L = \sqrt{\frac{Pr}{Ra}} \frac{Ma}{\sqrt{3}} \frac{1}{\delta_x}, \quad \alpha_L = \frac{\nu_L}{Pr} \quad \text{and} \quad \delta_t = \frac{Ma}{\sqrt{3}} \delta_x \tag{39}$$

The parameters are now Ra, Pr, $\delta_x = 1/N_x$ and the Mach number Ma. The time step varies linearly with Ma as shown in the previous relation. All parameters are then known and it is convenient to chose $Ma < 0.3$ to make sure the flow stays in the incompressible regime.

In practical, with the MRT formulation, the coefficient a is first set through the relation $a = 20Ma/\delta_x\sqrt{RaPr} - 4$. In order to avoid numerical instability of the $d2q5$ model, the value of a must be kept such as $a < 1$ (13; 41).

4 Results and discussion

System (1) is solved with the double MRT thermal lattice Boltzmann formulation for two configurations. In a first part we present a classical validation test case: the square cavity with $Ra = 10^6$. In a second part, we study a periodic flow obtained for the 8:1 aspect ratio cavity and $Ra = 3.4 \times 10^5$. Convergence orders and extrapolated values are then computed by the Richardson extrapolation. In both cases the Prandtl number is $Pr = 0.71$.

4.1 Richardson Extrapolation

In order to check the numerical convergence and the order of the numerical scheme, the Richardson Extrapolation (RE) is used. Detailed principles and assumptions can be found in (36). RE is constructed with Taylor expansion and then supposes sufficiently smooth exact solution f_{exact}. Small space (or time) step must be small enough so that the discrete solution f_{h_i} is in the convergence region. The general principle of RE consists of computing numerical solutions of the discretized problem on N different uniform grids of size h_i, with h_1 the coarsest grid and h_N the finest one. The solution for the mesh h_i is written in the form

$$f_{h_i} = f_{exact} + C_\alpha h_i^\alpha + \mathcal{O}(h_i^{\alpha+1}) \tag{40}$$

where C_α is a coefficient. Thus, by using three grids ($N = 3$) such as $h_1/h_2 = h_2/h_3$, the approximations $\tilde{\alpha}$, $\tilde{C}_\alpha$ and $\tilde{f}^{extra}$ are given by

$$\begin{aligned} \tilde{\alpha} &= \frac{\ln[(f_{h_1} - f_{h_2})/(f_{h_2} - f_{h_3})]}{\ln(h_1/h_2)} \\ \tilde{C}_\alpha &= \frac{f_{h_2} - f_{h_3}}{h_2^{\tilde{\alpha}} - h_3^{\tilde{\alpha}}} \\ \tilde{f}^{extra} &= f_{h_3} - \tilde{C}_\alpha h_3^{\tilde{\alpha}} \end{aligned} \tag{41}$$

with $\tilde{C}_\alpha = C_\alpha + \mathcal{O}(h_{N-1})$ and $\tilde{f}^{extra} = f_{exact} + \tilde{C}_\alpha h_N^{\tilde{\alpha}+1}$. As a consequence, the approximation $\tilde{f}^{extra}$ will be closer to the asymptotic solution f_{exact} with decreasing h_N and increasing $\tilde{\alpha}$. In practical, the use of RE under good conditions increases of one order the numerical solution. In this paper, RE is used with $N = 3$ and $N = 4$ such as $h_1/h_2 = h_2/h_3$ and $h_1/h_2 = h_3/h_4$ respectively (see Ref. (36) for the $N = 4$ case). Since RE is based on Taylor expansion, the same principle can be applied to temporal convergence.

4.2 Steady flow

In this section, the aspect ratio is fixed to the unity. The Rayleigh number is $Ra = 10^6$. This configuration has been extensively studied with various numerical methods (7; 27; 16). Here we will use the spectral results of Le Quéré (27) as a comparison for the quantities of interest. To our knowledge, Le Quéré provides the most accurate values in the literature.

For this benchmark, we need to compute the following quantities: the maximum horizontal velocity at mid-height $u_{\max} = \max(u(x, y = A/2))$, the maximum vertical velocity at mid-width $v_{\max} = \max(v(x = A/2, y))$ and their respective positions $y_{\max}$ and $x_{\max}$. These values are then scaled with the diffusive velocity α/W. The Nusselt number Nu and the averaged Nusselt number $\overline{Nu}$ are calculated at the hot wall:

$$Nu(y) = -\frac{1}{\theta_h - \theta_c} \left.\frac{\partial\theta}{\partial x}\right|_{wall} \tag{42}$$

and

$$\overline{Nu} = \frac{1}{H}\int_0^H Nu(y)\,dy \tag{43}$$

Integral calculations are performed with a second-order accuracy Newton-Cotes quadrature (trapezoid or mid-point rule). Positions of maximum and minimum Nusselt values at the hot wall are also estimated. The steady flow is assumed converged when the following criteria is reached:

$$\frac{\sum_{i=1}^{9}\sum_{j=1}^{N_x\times N_y} ||f_i(\boldsymbol{x}_j, t+100\,\delta_t) - f_i(\boldsymbol{x}_j, t)||_1}{\sum_{i=1}^{9}\sum_{j=1}^{N_x\times N_y} ||f_i(\boldsymbol{x}_j, t+100\,\delta_t)||_1} \leq 10^{-9} \tag{44}$$

where $||\cdot||_1$ denotes the L_1 norm.

The Mach number is set to $Ma = 5\times10^{-2}$. It has been shown (41) that there is no influence of the Mach number in this stationary problem. Tables 1 and 2 shows the numerical results for BB-BCs and ZHCS-BCs respectively.

At first, using finer grids makes the values converge through the expected ones. On the finer grid, $N_x \times N_y = 301^2$, the maximum difference is less than 2% for the BB-BCs and less than 1% for ZHCS-BCs. However, this difference is not significant. We can notice that some quantities do not converge through Le Quéré ones. For example, the extrapolated value x of the maximum vertical velocity is slightly greater than the reference.

Thanks to the RE, extrapolated values and convergence order are computed. The convergence orders are quite acceptable for both boundary conditions sets. The second-order convergence (here with space step) is obtained for most of the quantities of interest. The use of three and four points shows that the convergence region seems to be larger for the ZHCS-BCs formulation.

We would like to underline that the use of a single time relaxation model for the temperature (BGK) does not change results in a significant way.

To sum up, these observations are in good agreement with references. Both boundary conditions approaches lead to the expected results. The relative difference between the two implementations is less than 0.5%. Furthermore, the correct convergence orders validate our implementation and allows us to simulate a time-dependent natural convection case.

4.3 Periodic flow

In this section, the 8:1 aspect ratio differentially heated cavity is simulated. As presented in (43; 6), with the Rayleigh number $Ra = 3.4\times10^5$, the flow admits only one time-dependent skew-symmetric solution. This configuration has been studied by multiple authors and stands for a benchmark for time-dependent natural convection. A synthesis can be found in (6).

Two probes are set in the cavity. Their respective coordinates are $(x_1, y_1) = (0.1810, 7.3700)$ and $(x_2, y_2) = (0.8190, 7.3700)$. The quantities under study

are mean values of horizontal velocity $\overline{u}$ and temperature $\overline{\theta}$ at probe position 1, mean value of pressure difference between points 1 and 2 $\overline{\Delta p}_{12}$, mean value of the Nusselt number $\overline{Nu}$ at hot wall and their respective perturbations u', θ', $\Delta p'_{12}$, Nu'. The pressure is obtained through the relation $p = \rho c_s$. For a quantity ϕ, the mean value $\overline{\phi}$ and the oscillatory component ϕ' are computed as:

$$\overline{\phi} = \frac{1}{\tau} \int_t^{t+\tau} \phi(\boldsymbol{x}, t)\, dt \tag{45}$$

and

$$\phi' = \max(\phi(\boldsymbol{x}, t)) - \min(\phi(\boldsymbol{x}, t)) \tag{46}$$

where τ represents the period (based on temperature evolution at probe 1) for which the average is computed.

The dimensionless temperature evolution is given in figure 2 while iso-lines of the temperature field over one period are presented in figure 3. The temperature field is stratified in the center while oscillations are visible at the top and the bottom of the cavity. At first sight, a single frequency time-dependent flow is observed. The periodic state is reached for dimensionless times greater than 600. Quantities of interest are extracted during a period τ for times greater than 1000.

Tables 3 and 4 present the evolution quantities of interest for different meshes with $Ma = 0.1$. The reference values of Xin and Le Quéré (43) for this problem are also given as the results of the RE on three and four meshes.

First, the mean values approach the reference for both boundary conditions sets except the pressure difference $\overline{\Delta p}_{12}$ in the case of BB-BCs (Tab. 3). Unlike most quantities, the relative difference on $\overline{\Delta p}_{12}$ obtained on coarse grids is important (78%). Even for the finest grids, it remains greater than 20%. For this particular variable, the RE produces nearly a first accuracy space convergence order ($\tilde{\alpha} = 0.74$ and 0.82 respectively with three and four meshes). With ZHCS-BBs (Tab. 4), the difference is smaller and acceptable. It decreases form 12% to 1.5% and a second order accuracy convergence is obtained ($\tilde{\alpha} \simeq 2.1$).

Secondly, the oscillatory values do not converge through the reference and present a non negligible relative difference. With the finest meshes, almost a 5% difference is obtained. As shown in table 5 for BB-BCs, this behaviour is linked to the Mach number (or the time step). The decreasing time step makes the values converge and, with the smallest Mach number $Ma = 0.05$, their relative difference is about 2%. On the other side, the correct mean values are obtained even for large Mach number. This observation is consistent with the Mach number independence for stationary data.

Finally, the convergence orders are discussed (Tab. 5). With space step, RE shows that theoretical predicted orders are better recovered with ZHCS-BCs approach. Like in the pressure field case, space convergence orders for the mean velocity $\overline{u}_1$ and temperature $\overline{\theta}_1$ are close to the unity with the BB-BCs approach. With ZHCS-BBs, the second-order accuracy is obtained for most quantities, mean value and oscillatory component. An explanation could be that when bounce-back conditions are used, the grid is not totally regular: the wall is half

a space-step beyond the last fluid node. Hence, the condition of regular grid for the RE is not fulfilled when BB-BCs are applied. With time step, analysis on mean values provides a second-order accuracy except for the Nusselt number. We suppose this quantity outside the convergence region. The theoretical order is also recovered for oscillatory data. It is important to notice that the choice of the boundary condition formulation does not change the temporal convergence order.

We notice that simulations were also performed with the simplified $d2q9$ internal energy thermal model for temperature introduced in (37). The results on finer meshes are quite close to those obtained with the double MRT approach. But, as it is based on a single relaxation time, simulations are unstable for small relaxation rates, typically less than 0.55, and a rigorous convergence study is not possible as it requires too important meshes. We should emphasize that this problem is very expensive to simulate and a parallel implementation is highly recommended. As mentioned in Sec. 3.5, the time step varies linearly with both space step and Mach number. For guidance, time calculations are given in table 5 as a function of the Mach number. Calculation times could probably be reduced using a mesh refinement algorithm developed for non uniform grids (19; 38). In this paper, regular meshes are uses as required for the Richardson extrapolation.

To summarize this section, predicted results and convergence orders were obtained for a periodic thermal flow. As expected, the Mach number is a crucial parameter in time-dependent problem. When the pressure field is a relevant quantity, ZHCS-BCs approach gives better results and should be used.

5 Conclusion

In this paper, the double multiple-relaxation-time collision model for the lattice Boltzmann equation has been implemented to simulate two natural convection problems under the Boussinesq assumption. Two kinds of popular boundary conditions have been tested. The bounce-back approach where walls are halfway beyond the last fluid node, and a "on-node" approach constructed with Zou and He and Counter-Slip formulations. The Richardson extrapolation has systematically been used to compute an extrapolated solution and convergence orders from the numerical results.

The results are in good agreement with reference benchmark studies. The double MRT method is numerically more stable than double BGK or MRT-BGK formulations and thus allows rigorous convergence studies. With the finest space and time steps, less than 1% relative difference error is observed for most of the quantities of interest. The non-negligible error made on the pressure field and the small convergence order obtained with bounce-back conditions are corrected with the "on-node" formulation. The latter provides a better framework to study numerical properties. It should be used when the pressure field is a relevant quantity. The time-dependent flow study highlights the significant effect of the Mach number, or time step, on the oscillatory data. The expected

second-order time accuracy has been found for both mean and oscillatory values and makes the multiple-relaxation-time thermal lattice Boltzmann model suitable for time-dependent thermal flows.

References

[1] F. J. Alexander, S. Chen, and J. D. Sterling. Lattice Boltzmann thermohydrodynamics. *Phys. Rev. E*, 47:2249–2252, 1993.

[2] H. R. Ashorynejad, A. A. Mohamad, M. Sheikholeslami. Magnetic field effects on natural convection flow of a nanofluid in a horizontal cylindrical annulus using Lattice Boltzmann method. *Int. J. Therm. Sci.*, 64:240–250, 2013.

[3] P. L. Bhatnagar, E. P. Gross, and M. Krook. A Model for Collision Processes in Gases. I. Small Amplitude Processes in Charged and Neutral One-Component Systems. *Phys. Rev.*, 94:511–525, 1954.

[4] M. Bouzidi, M. Firdaouss, and P. Lallemand. Momentum transfer of a Boltzmann-lattice fluid with boundaries. *Phys. Fluids*, 13:3452–3459, 2001.

[5] S. Chen and G. D. Doolen. Lattice Boltzmann method for fluid flows. *Annu. Rev. Fluid Mech.*, 30:329–364, 1998.

[6] M. A. Christon, P. M. Gresho, and S. B. Sutton. Computational predictability of time-dependent natural convection flows in enclosures (including a benchmark solution). *Int. J. Numer. Meth. Fl.*, 40:953–980, 2002.

[7] G. de Vahl Davis. Natural convection in air square cavity: a benchmark numerical solution. *Int. J. Numer. Meth. Fl.*, 3:249–264, 1983.

[8] D. d'Humières, I. Ginzburg, M. Krafczyk, P. Lallemand, and L.-S. Luo. Multiple-Relaxation-Time Lattice Boltzmann Models in Three Dimensions. *Philos. T. R. Soc. A*, 360:437–451, 2002.

[9] H. Dixit and V. Babu. Simulation of high Rayleigh number natural convection in a square cavity using the lattice Boltzmann method. *Int. J. Heat Mass Tran.*, 49:727–739, 2006.

[10] A. D'Orazio, M. Coricone, and G. P. Celata. Application to natural convection enclosed flows of a lattice Boltzmann BGK model coupled with a general purpose thermal boundary condition. *Int. J. Therm. Sci.*, 43:575–586, 2004.

[11] A. D'Orazio and S. Succi. *Computational Science – ICC 2003*, chapter Boundary Conditions for Thermal Lattice Boltzmann Simulations, pages 977–986. Springer Berlin Heidelberg, 2003.

[12] U. Frisch, D. d'Humières, B. Hasslacher, P. Lallemand, Y. Pomeau, and J.-P. Rivet. Lattice gas hydrodynamics in two and three dimensions. *Complex Syst.*, 1:649–707, 1987.

[13] I. Ginzburg, D. d'Humières, and A. Kuzmin. Optimal stability of advection-diffusion lattice Boltzmann models with two relaxation times for positive/negative equilibrium. *J. Stat. Phys.*, 139(6):1090–1143, 2010.

[14] I. Ginzburg and D. d'Humières. Multireflexion boundary conditions for Lattice Boltzmann models. *Phys. Rev. E*, 68:066614, 2003.

[15] I. Ginzburg, F. Verhaeghe, and D. d'Humières. Two-relaxation-time lattice Boltzmann scheme: about parametrization, velocity, pressure and mixed boundary conditions. *Commun. Comput. Phys.*, 3:427–478, 2008.

[16] Z. Guo, B. Shi, and C. Zheng. A coupled lattice bgk model for the boussinesq equations. *Int. J. Numer. Meth. Fl.*, 39(4):325–342, 2002.

[17] X. He and L.-S. Luo. Lattice Boltzmann Model for the Incompressible Navier-Stokes Equation. *J. Stat. Phys.*, 88:927–944, 1997.

[18] X. He, S. Chen, and G. D. Doolen. A novel thermal model for the lattice Boltzmann method in incompressible limit. *J. Comput. Phys.*, 146(1):282 –300, 1998.

[19] X. He, L.-S. Luo, and M. Dembo. Some Progress in Lattice Boltzmann Method. Part I. Nonuniform Mesh Grids. *J. Comput. Phys.*, 129:357–363, 1996.

[20] H.-B. Huang, X.-L. Lu, and M. C. Sukop. Numerical study of lattice Boltzmann methods for a convection-diffusion equation coupled with Navier–Stokes equations. *J. Phys. A-Math. Theor.*, 44:055001, 2011.

[21] T. Inamuro, M. Yoshina, and F. Ogino. A non-slip boundary condition for lattice Boltzmann simulations. *Phys. Fluids*, 7:2928–2930, 1995.

[22] M. Jami, A. Mezrhab, M. Bouzidi, and P. Lallemand. Lattice Boltzmann method applied to the laminar natural convection in an enclosure with a heat-generating cylinder conducting body. *Int. J. Therm. Sci.*, 46(1):38–47, 2007.

[23] P. Lallemand and L.-S. Luo. Theory of the lattice Boltzmann method: Dispersion, dissipation, isotropy, galilean invariance, and stability. *Phys. Rev. E*, 61:6546–6562, Jun 2000.

[24] P. Lallemand and L.-S. Luo. Theory of the lattice Boltzmann method: Acoustic and thermal properties in two and three dimensions. *Phys. Rev. E*, 68:036706, Sep 2003.

[25] J. Latt. Choice of units in lattice Boltzmann simulations. 2008.

[26] J. Latt, B. Chopard, O. Malaspinas, M. Deville, and A. Michler. Straight velocity boundaries in the lattice Boltzmann method. *Phys. Rev. E*, 77:056703, 2008.

[27] P. Le Quéré. Accurate solutions to the square thermally driven cavity at hight rayleigh number. *Comput. Fluids*, 20:29–41, 1991.

[28] L.-S. Luo, W. Lao, X. Chen, Y. Peng, and W. Zhang. Numerics of the lattice Boltzmann method: Effects of collision models on the lattice Boltzmann simulations. *Phys. Rev. E*, 83:056710, 2011.

[29] G. R. McNamara and G. Zanetti. Use of the Boltzmann equation to simulate lattice-gas automata. *Phys. Rev. Lett.*, 61:2332–2335, Nov 1988.

[30] F. Meng, M. Wang, and Z. Li. Lattice Botlzmann simulations of conjugate hear transfer in high-frequency oscillating flows. *Int. J. Heat. Fluid Fl.*, 29:1203–1210, 2008.

[31] A. Mezrhab, M. Bouzidi, and P. Lallemand. Hybrid lattice-Boltzmann finite-difference simulation of convective flows. *Comput. Fluids*, 33(4):623–641, 2004.

[32] A. Mezrhab, M. A. Moussaoui, M. Jami, H. Naji, and M. Bouzidi. Double MRT thermal lattice Boltzmann method for simulating convective flows. *Phys. Lett. A*, 374(34):3499–3507, 2010.

[33] A. A. Mohamad and A. Kuzmin. A critical evaluation of force term in lattice Boltzmann method, natural convection problem. *Int. J. Heat Mass Tran.*, 53:990–996, 2010.

[34] A. A. Mohamad. Lattice Boltzmann Methods, Fundamentals, Applications, with Computer Codes *Springer*, 2011.

[35] M. Moussaoui, A. Mezrhab, and H. Naji. A computation of flow and heat transfer past three heated cylinders in a vee shape by a double distribution MRT thermal lattice Boltzmann model. *Int. J. Therm. Sci.*, 50(8):1532–1542, 2011.

[36] X. Nicolas, S. Gounand, M. Médale, and S. Glockner. Benchmark Solution for a Three-Dimensional Mixed-Convection Flow, Part 2: Analysis of Richardson Extrapolation in the Presence of a Singularity. *Numer. Heat Tr. B-Fund.*, 60:346–369, 2011.

[37] Y. Peng, C. Shu, and Y. Chew. Simplified thermal lattice Boltzmann model for incompressible thermal flows. *Phys. Rev. E*, 68:026701, 2003.

[38] C. Shu, Y. Peng, and Y. Chew. Simulation of natural convection in square cavity by Taylor series expansion- and least squares-based lattice Boltzmann method. *Int. J. Mod. Phys. C*, 13:1399–1414, 2002.

[39] G. Silva. Corner boundary conditions in lattice Boltzmann method. Lecture note, 2011.

[40] S. Suga. Numerical schemes obtained from lattice Boltzmann equations for advection diffusion equations. *Int. J. Mod. Phys. C*, 17:1563, 2006.

[41] J. Wang, D. Wang, P. Lallemand, and L.-S. Luo. Lattice Boltzmann simulation of thermal convective flows in two dimensions. *Comput. Math. Appl.*, 65:262–286, 2013.

[42] J. Wang, M. Wang, and Z. Li. A lattice Boltzmann algorithm for fluid-solid conjugate heat transfer. *Int. J. Therm. Sci.*, 46(3):228–234, 2007.

[43] S. Xin and P. Le Quéré. An extended Chebychev pseudo-spectral benchmark for the 8:1 differentially heated cavity. *Int. J. Numer. Meth. Fl.*, 40:981–998, 2002.

[44] Y. Yan and Y. Zu. Numerical simulation of heat transfer and fluid flow past a rotating isothermal cylinder - A LBM approach. *Int. J. Heat Mass Tran.*, 51(910):2519–2536, 2008.

[45] Q. Zou and X. He. On pressure and velocity boundary conditions for the lattice Boltzmann BGK model. *Phys. Fluids*, 9:1591–1598, 1997.

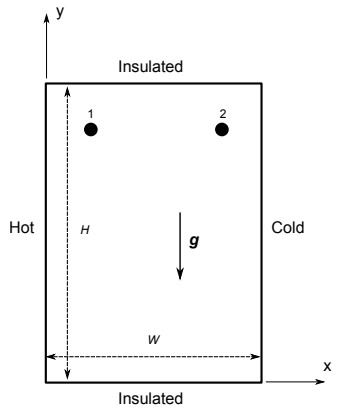

Figure 1: Differentially heated cavity with insulated horizontal walls and constant temperature vertical walls. The aspect ratio is $A = H/W$. Points 1 and 2, respectively in (x_1, y_1) and (x_2, y_2), are time history points.

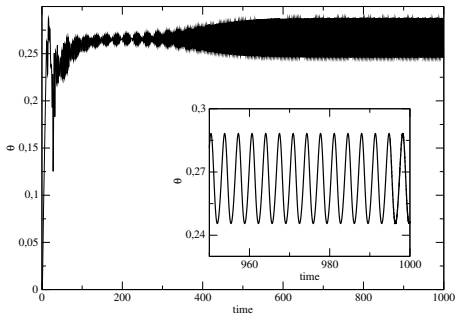

Figure 2: Dimensionless temperature θ as a function of time at probe $(x_1, y_1) = (0.1810, 7.3700)$

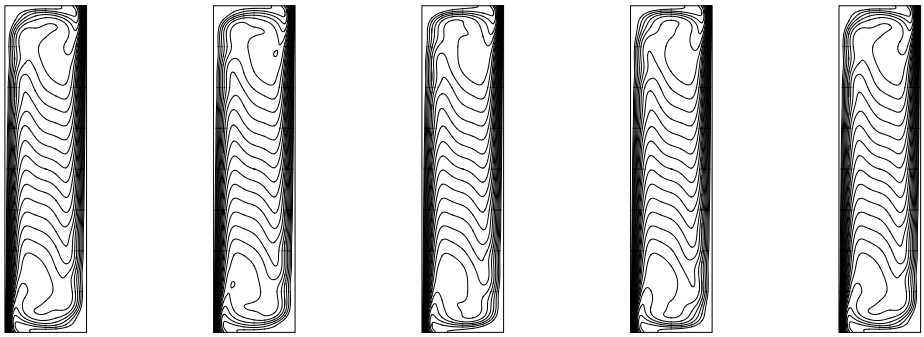

Figure 3: Iso-lines of temperature (difference between two iso-lines: $\delta T = 3.84 \times 10^{-2}$) over one period τ. Left to right $t = 0, \tau/4, \tau/2, 3\tau/4, \tau$. $Ra = 3.4 \times 10^5$, $Pr = 0.71$, $Ma = 10^{-1}$ and $N_x \times N_y = 301 \times 2401$.

$N_x \times N_y$	$u_{\max}$	y	$v_{\max}$	x
75^2	64.7722(0.10%)	0.8484(0.18%)	220.907(0.16%)	0.03791(0.24%)
100^2	64.7999(0.05%)	0.8491(0.10%)	220.772(0.10%)	0.03786(0.37%)
150^2	64.8216(0.02%)	0.8496(0.04%)	220.658(0.04%)	0.03780(0.53%)
200^2	64.8279(0.01%)	0.8498(0.02%)	220.625(0.03%)	0.03779(0.55%)
300^2	64.8264(0.01%)	0.8503(0.05%)	220.620(0.03%)	0.03777(0.61%)
Ref (27)	64.8344	0.8500	220.559	0.03800
$\tilde{f}^{extra}_{N=3}(\tilde{\alpha})$	64.8269(3.36)	0.8517(0.65)	220.613(2.71)	0.03792(1.88)
$\tilde{f}^{extra}_{N=4}(\tilde{\alpha})$	64.8361(1.97)	0.8500(1.94)	220.577(1.83)	0.03773(1.60)
$N_x \times N_y$	$\overline{Nu}$	$Nu_{\max}$	y	$Nu_{\min}$
75^2	8.9612(1.54%)	19.5679(11.6%)	0.0473(21.3%)	0.81666(16.6%)
100^2	8.8980(0.83%)	18.6947(6.61%)	0.0428(9.78%)	0.90300(7.81%)
150^2	8.8544(0.33%)	18.0240(2.78%)	0.0398(2.05%)	0.96117(1.87%)
200^2	8.8403(0.17%)	17.7955(1.48%)	0.0391(0.32%)	0.97732(0.22%)
300^2	8.8310(0.07%)	17.6419(0.60%)	0.0383(1.54%)	0.98440(0.50%)
Ref (27)	8.8252	17.5360	0.0390	0.97946
$\tilde{f}^{extra}_{N=3}(\tilde{\alpha})$	8.8245(2.19)	17.5162(2.01)	0.03807(2.42)	0.9888(2.63)
$\tilde{f}^{extra}_{N=4}(\tilde{\alpha})$	8.8237(2.13)	17.4770(1.87)	0.03847(2.47)	0.9944(2.31)

Table 1: Convergence of values with $Pr = 0.71$, $Ra = 10^6$ and $Ma = 5 \times 10^{-2}$ for BB-BCs. The reference values of Le Quéré (27) are also presented as the results of RE on three ($N = 3$) and four ($N = 4$) meshes. Values in parenthesis are relative differences with reference or convergence order.

$N_x \times N_y$	$u_{\max}$	y	$v_{\max}$	x
76^2	64.2827(0.85%)	0.8513(0.16%)	218.983(0.71%)	0.03893(2.46%)
101^2	64.5255(0.48%)	0.8507(0.08%)	219.734(0.37%)	0.03842(1.12%)
151^2	64.6988(0.21%)	0.8503(0.04%)	220.206(0.16%)	0.03807(0.18%)
201^2	64.7601(0.11%)	0.8501(0.02%)	220.372(0.08%)	0.03793(0.18%)
301^2	64.8010(0.05%)	0.8500(0.00%)	220.482(0.03%)	0.03778(0.57%)
Ref (27)	64.8344	0.8500	220.559	0.03800
$\tilde{f}^{extra}_{N=3}(\tilde{\alpha})$	64.8342(2.02)	0.8498(1.62)	220.562(2.14)	0.03764(1.61)
$\tilde{f}^{extra}_{N=4}(\tilde{\alpha})$	64.8393(1.99)	0.8500(2.21)	220.553(2.26)	0.03774(1.95)
$N_x \times N_y$	$\overline{Nu}$	$Nu_{\max}$	y	$Nu_{\min}$
76^2	8.8362(0.13%)	18.0556(2.96%)	0.0460(17.5%)	0.82666(15.6%)
101^2	8.8244(0.01%)	17.8409(1.74%)	0.0426(9.37%)	0.90280(7.83%)
151^2	8.8161(0.10%)	17.6769(0.80%)	0.0403(3.36%)	0.96224(1.76%)
201^2	8.8139(0.13%)	17.6226(0.49%)	0.0395(1.49%)	0.97792(0.16%)
301^2	8.8128(0.14%)	17.5853(0.28%)	0.0393(0.91%)	0.98542(0.61%)
Ref (27)	8.8252	17.5360	0.0390	0.97946
$\tilde{f}^{extra}_{N=3}(\tilde{\alpha})$	8.8121(2.59)	17.5562(2.04)	0.0391(2.57)	0.99019(2.54)
$\tilde{f}^{extra}_{N=4}(\tilde{\alpha})$	8.8114(2.25)	17.5488(1.91)	0.0387(2.12)	0.99742(2.05)

Table 2: Convergence of values with $Pr = 0.71$, $Ra = 10^6$ and $Ma = 5 \times 10^{-2}$ for ZHCS-BCs. The reference values of Le Quéré (27) are also presented as the results of RE on three ($N = 3$) and four ($N = 4$) meshes. Values in parenthesis are relative differences with reference or convergence order.

$N_x \times N_y$	$\overline{u}_1$	$\overline{\theta}_1$	$\overline{Nu}$	$\overline{\Delta p}_{12}$	τ
75×600	0.052258(7.27%)	0.265875(0.15%)	4.594463(0.33%)	0.000394(78.7%)	3.433715(0.65%)
100×800	0.053549(4.98%)	0.265787(0.12%)	4.587082(0.17%)	0.000709(61.7%)	3.425231(0.40%)
150×1200	0.054752(2.85%)	0.265701(0.08%)	4.582309(0.06%)	0.001065(42.4%)	3.418987(0.22%)
200×1600	0.055291(1.89%)	0.265651(0.06%)	4.580837(0.03%)	0.001251(32.4%)	3.417280(0.17%)
300×2400	0.055794(1.00%)	0.265598(0.04%)	4.579920(0.01%)	0.001443(22.0%)	3.415954(0.13%)
Ref (43)	0.056356	0.265480	4.579460	0.001850	3.41150
$\tilde{f}^{extra}_{N=3}(\tilde{\alpha})$	0.056541(1.25)	0.265448(0.75)	4.579335(2.34)	0.001930(0.82)	3.415167(2.27)
$\tilde{f}^{extra}_{N=4}(\tilde{\alpha})$	0.056539(1.24)	0.265472(0.85)	4.579281(2.31)	0.002032(0.74)	3.415277(2.14)
$N_x \times N_y$	u'_1	θ'_1	Nu'	$\Delta p'_{12}$	
75×600	0.050830(7.29%)	0.039788(6.91%)	0.006336(10.8%)	0.018641(8.53%)	
100×800	0.054594(0.43%)	0.042632(0.25%)	0.006860(3.38%)	0.020011(1.81%)	
150×1200	0.056746(3.50%)	0.044221(3.47%)	0.007173(1.03%)	0.020817(2.14%)	
200×1600	0.057327(4.56%)	0.044617(4.39%)	0.007261(2.27%)	0.021052(3.30%)	
300×2400	0.057572(5.00%)	0.044753(4.71%)	0.007307(2.92%)	0.021175(3.90%)	
Ref (43)	0.054828	0.042740	0.007100	0.020380	
$\tilde{f}^{extra}_{N=3}(\tilde{\alpha})$	0.0577060(2.84)	0.0448256(3.05)	0.0073325(2.64)	0.0212455(2.60)	
$\tilde{f}^{extra}_{N=4}(\tilde{\alpha})$	0.0578259(2.68)	0.0449381(2.79)	0.0073419(2.55)	0.0212675(2.56)	

Table 3: Convergence of values with $Pr = 0.71$, $Ra = 3.4 \times 10^5$ and $Ma = 10^{-1}$ for BB-BCs. The reference values of Xin and Le Quéré (43) are also presented as the results of RE on three ($N = 3$) and four ($N = 4$) meshes. Values in parenthesis are relative differences with reference or convergence order.

$N_x \times N_y$	$\overline{u}_1$	$\overline{\theta}_1$	$\overline{Nu}$	$\overline{\Delta p}_{12}$	τ
76×601	0.057049(1.23%)	0.265821(0.13%)	4.591869(0.27%)	0.001621(12.3%)	3.441009(0.86%)
101×801	0.056936(1.03%)	0.265701(0.08%)	4.586808(0.16%)	0.001717(7.19%)	3.430037(0.54%)
151×1201	0.056838(0.86%)	0.265621(0.05%)	4.583163(0.08%)	0.001785(3.51%)	3.421374(0.29%)
201×1601	0.056818(0.82%)	0.265586(0.04%)	4.582049(0.06%)	0.001806(2.38%)	3.418490(0.20%)
301×2401	0.056794(0.78%)	0.265557(0.03%)	4.581215(0.04%)	0.001823(1.46%)	3.416565(0.15%)
Ref (43)	0.056356	0.265480	4.579460	0.001850	3.411500
$\tilde{f}^{extra}_{N=3}(\tilde{\alpha})$	0.056782(2.26)	0.265527(1.64)	4.580653(2.16)	0.001834(2.11)	3.415005(2.03)
$\tilde{f}^{extra}_{N=4}(\tilde{\alpha})$	0.056793(2.02)	0.265539(1.92)	4.580706(2.10)	0.001831(2.12)	3.414373(1.85)
$N_x \times N_y$	u'_1	θ'_1	Nu'	$\Delta p'_{12}$	
76×601	0.051456(6.15%)	0.039804(6.87%)	0.006324(10.9%)	0.018610(8.68%)	
101×801	0.054653(0.32%)	0.042257(1.13%)	0.006793(4.32%)	0.020167(1.05%)	
151×1201	0.056912(3.80%)	0.044062(3.09%)	0.007132(0.45%)	0.020983(2.96%)	
201×1601	0.057483(4.84%)	0.044520(4.16%)	0.007232(1.86%)	0.021193(3.99%)	
301×2401	0.057689(5.22%)	0.044698(4.58%)	0.007289(2.66%)	0.021279(4.41%)	
Ref (43)	0.054828	0.042740	0.007100	0.020380	
$\tilde{f}^{extra}_{N=3}(\tilde{\alpha})$	0.057818(2.81)	0.044810(2.74)	0.007327(2.36)	0.021321(3.00)	
$\tilde{f}^{extra}_{N=4}(\tilde{\alpha})$	0.058098(2.28)	0.045040(2.20)	0.007351(2.12)	0.021353(2.91)	

Table 4: Convergence of values with $Pr = 0.71$, $Ra = 3.4 \times 10^5$ and $Ma = 10^{-1}$ for ZHCS-BCs. The reference values of Xin and Le Quéré (43) are also presented as the results of RE on three ($N = 3$) and four ($N = 4$) meshes. Values in parenthesis are relative differences with reference or convergence order.

Ma	$\overline{u}_1$	$\overline{\theta}_1$	$\overline{Nu}$	$\overline{\Delta p}_{12}$	τ
0.2	0.057180(1.46%)	0.265746(0.10%)	4.579715(0.01%)	0.001384(25.1%)	3.426895(0.45%)
0.1	0.055794(1.00%)	0.265598(0.04%)	4.579920(0.01%)	0.001443(22.0%)	3.415954(0.13%)
0.05	0.055468(1.58%)	0.265558(0.03%)	4.580093(0.01%)	0.001456(21.3%)	3.413460(0.06%)
Ref (43)	0.056356	0.265480	4.579460	0.001850	3.411500
$\tilde{f}^{extra}_{N=3}(\tilde{\alpha})$	0.055368(2.09)	0.265543(1.89)	4.581028(0.24)	0.001460(2.18)	3.412724(2.13)
Ma	u'_1	θ'_1	Nu'	$\Delta p'_{12}$	Cpu time (h)
0.2	0.066978(22.1%)	0.050714(18.6%)	0.007989(12.5%)	0.023792(16.7%)	1700
0.1	0.057572(5.00%)	0.044753(4.71%)	0.007307(2.92%)	0.021175(3.90%)	3350
0.05	0.055209(2.04%)	0.043100(0.84%)	0.007114(0.20%)	0.020418(0.19%)	7480
Ref (43)	0.054828	0.042740	0.007100	0.020380	-
$\tilde{f}^{extra}_{N=3}(\tilde{\alpha})$	0.054416(1.99)	0.042466(1.85)	0.007004(1.85)	0.020083(1.79)	-

Table 5: Convergence of values with $Pr = 0.71$, $Ra = 3.4 \times 10^5$ and $N_x \times N_y = 300 \times 2400$ for BB-BCs. The reference values of Xin and Le Quéré (43) are also presented as the results of RE on three ($N = 3$) meshes. Values in parenthesis are relative differences with reference or convergence order. For guidance, the total cpu time in hours on AMD 6276 computers is given.